

Article

On Agreement of Experimental Data and Calculated Results in Grain Boundary Segregation

Miroslav Černý^{1,2,*}, Petr Šesták^{1,2}, Monika Všianská^{1,3} and Pavel Lejček^{1,4}

¹ Central European Institute of Technology, CEITEC BUT, Brno University of Technology, Purkyňova 123, 612 69 Brno, Czech Republic

² Faculty of Mechanical Engineering, Brno University of Technology, Technická 2896/2, 616 69 Brno, Czech Republic

³ Department of Chemistry, Faculty of Science, Masaryk University, Kotlářská 2, 611 37 Brno, Czech Republic

⁴ Institute of Physics, Academy of Sciences of the Czech Republic, Na Slovance 2, 182 21 Prague, Czech Republic

* Correspondence: mcerny@vutbr.cz; Tel.: +420-541-142-709

Abstract: There are two sources of quantitative data on grain boundary segregation: careful experimental results and calculated data. These values can be compared in various ways. Here we show a comparison of average concentrations of silicon, vanadium, and tin at the grain boundaries of bcc iron determined in three ways: (i) on the basis of calculations of the segregation energy for individual sites; (ii) experimentally; and (iii) using a phenomenological prediction for selected systems characterized by satisfactory solid solubility of the segregant in bulk. We found very good agreement between the results of these approaches for all three of the segregants. The results clearly show the indispensable role of so-called ‘anti-segregation sites’ in the determination of average grain boundary concentration as well as the importance of segregation entropy and consequently, of entropy-dominated grain boundary segregation.

Keywords: DFT calculations; experimental data; energy; entropy; grain boundaries; machine learning; segregation



Citation: Černý, M.; Šesták, P.; Všianská, M.; Lejček, P. On Agreement of Experimental Data and Calculated Results in Grain Boundary Segregation. *Metals* **2022**, *12*, 1389. <https://doi.org/10.3390/met12081389>

Academic Editor: Philip Eisenlohr

Received: 25 July 2022

Accepted: 19 August 2022

Published: 21 August 2022

Publisher’s Note: MDPI stays neutral with regard to jurisdictional claims in published maps and institutional affiliations.



Copyright: © 2022 by the authors. Licensee MDPI, Basel, Switzerland. This article is an open access article distributed under the terms and conditions of the Creative Commons Attribution (CC BY) license (<https://creativecommons.org/licenses/by/4.0/>).

1. Introduction

The chemical composition of material interfaces, such as grain boundaries and free surfaces, usually differs significantly from that of crystal volumes. Foreign atoms accumulate at the interfaces, and consequently affect the materials’ properties [1–3]. A specific case of the interface is a grain boundary and its enrichment by solutes, also called grain boundary segregation [4].

The researchers have been seeking ways to determine the composition of the interfaces for decades. The first attempts to detect the chemistry of grain boundaries were represented by indirect methods, such as auto-radiography, changes in the surface energy of the grain boundaries, and hardness measurements [5]. Later, direct methods were developed for the quantitative analysis of the interfaces. Some of the direct methods are based on surface analysis, such as Auger electron spectroscopy, AES, and X-Ray photoelectron spectroscopy, XPS, with the latter sometimes called electron spectroscopy for chemical analysis, ESCA (all applied on fracture surfaces after brittle intergranular cracking [6]). Other methods are based on high-resolution electron microscopy and secondary ion mass spectroscopy (for a brief summary, see [3]). Recently, a lot of effort has been devoted to study of grain boundary segregation using 3D atom probe tomography, 3D APT [7,8]. The resolution of these methods is out of the atomic scale; however, the average concentration at the boundary can be determined. The application of the above-mentioned methods resulted in a large amount data, which enabled them to be generalized in some cases and for the enthalpy and entropy of grain boundary segregation to be determined [9].

Simultaneously, a number of attempts have been made to determine the energy of grain boundary segregation theoretically. Methods such as molecular statics, molecular dynamics, Monte Carlo, and most importantly those based on the density functional theory (DFT) were applied in these calculations [9]. A noticeable advantage of the DFT calculations is the possibility to calculate the segregation energy at individual boundary and surface sites. Unfortunately, the most frequently used DFT calculations can be only performed at 0 K and therefore, they do not allow the determination of the segregation entropy.

The comparison of the calculated results with the experimental data is not completely straightforward. The values of the segregation energy obtained in these different ways are well comparable when they are relatively low, i.e., for the solutes exhibiting high solid solubility [10]. On the other hand, values of the energy of grain boundary segregation of solutes with low solid solubility exhibit large scatter and usually do not fit with the experimentally determined ones [10]. Additionally, values of the segregation entropy are required for the complete determination of the grain boundary concentration. They can be estimated on the basis of the enthalpy–entropy compensation effect [11,12] (for more details, see Section 2, Equation (4)). The interpretation of this effect is also debatable, as recently Scheiber and Romaner [12] suggested a new interpretation of individual lines in the enthalpy–entropy diagram based on the width of the segregation energy spectrum of the grain boundaries. Their interpretation contrasts with the previous distinction of the lines on the basis of the segregation site, i.e., interstitial or substitutional [11].

In this paper we attempt to directly compare the grain boundary concentrations of selected solutes being well soluble in bcc iron. The values of these concentrations are determined using either the values of the segregation energy published in the literature, or the values of the enthalpy of grain boundary segregation estimated on the basis of the phenomenological model [9]. In both cases, the estimated values of the segregation entropy were also considered [11,12].

2. Determination of Grain Boundary Composition

As mentioned above, there are two ways to obtain the values of grain boundary concentration: (i) from experimental measurements of grain boundary segregation at individual temperatures which provide average grain boundary concentrations; and (ii) from theoretical calculations of the segregation energies at individual sites.

The grain boundary composition is usually measured by AES on grain boundary fracture surfaces opening the grain boundary [13]. The concentrations X_I^{GB} can be extracted from the Auger spectra by standardized methods as described, e.g., in Refs. [6,13]. If the measurements are conducted at various temperatures, we can draw the values of the enthalpy, ΔH_I , and entropy, ΔS_I , of grain boundary segregation of solute I in host M . In a more precise experiments, the values of the standard (ideal) segregation enthalpy, ΔH_I^0 , and entropy, ΔS_I^0 , together with the (Fowler) coefficient of I – I interaction in host M , $\alpha_{I(M)}$ [3], can be obtained:

$$X_I^{GB} = \frac{X_I \exp[-(\Delta H_I - T\Delta S_I)/RT]}{1 - X_I + X_I \exp[-(\Delta H_I - T\Delta S_I)/RT]}. \quad (1)$$

In Equation (1), X_I is the bulk concentration. The above-mentioned values fulfill the following relationship [3]:

$$\Delta H_I - T\Delta S_I = \Delta H_I^0 - T\Delta S_I^0 - 2\alpha_{I(M)}. \quad (2)$$

If a single grain boundary is measured, the values of ΔH_I^0 and ΔS_I^0 characterize this boundary (on average).

Based on numerous measurements of segregation at individual grain boundaries, some generalizations can be made. The first one follows the suggestion of Hondros and Seah [14]. An analysis shows that ΔH_I^0 depends on bulk solid solubility, $X_I^{V,*}$ by [15]:

$$\Delta H_I^0 = \Delta H_{CSS}^* + vR \left[T \ln X_I^{V,*}(T) \right], \quad (3)$$

with ΔH_{CSS}^* being the standard enthalpy of segregation of a completely solid-soluble (CSS) solute in M , and v being the parameter characteristic for the host. The product $T \ln X_I^{V,*}(T) \neq f(T)$, ΔH_I^0 is independent of temperature. For more details, see [15,16].

The other relationship represents the enthalpy–entropy compensation effect [16],

$$\Delta S_I^0 = \frac{\Delta H_I^0}{T_{CE}} + \Delta S', \quad (4)$$

where T_{CE} is the compensation temperature and $\Delta S'$ is the constant of entropic character. As the relationship (4) splits into two branches, it is supposed (based on the nature of the solutes fitting individual branches) that they describe the segregation of interstitial (upper branch) and substitutional (bottom branch) solutes [16]. Recently Scheiber and Romaner [12] suggested this splitting to be a consequence of the width of the spectrum of the segregation energies at individual sites of a particular grain boundary.

3. Calculations of Segregation Energies

The theoretical values of the segregation energy at individual grain boundary sites can be obtained from first principles employing the density functional theory (DFT) and its particular implementation in the code VASP [17,18]. We used the projector augmented waves method [19] and the exchange–correlation energy was evaluated within the generalized gradient approximation parametrized by Perdew, Burke, and Ernzerhof (PBE) [20]. The magnetic ordering of the Fe atom was considered using spin polarized calculations. The plane-wave cut-off energy was set to 400 eV and the first Brillouin zone was sampled using a $19 \times 6 \times 2$ Γ -centered Monkhorst-Pack mesh that corresponded to the DFT supercell with 60 atoms (in the case of impurity segregation in substitutional positions) and dimensions of $2.83 \times 8.96 \times 27.47$ Å, as illustrated in Figure 1. Atomic planes are numbered 1–8 and positions for interstitially segregated impurities (smaller circles) are labeled by 0. If the impurity atoms occupy interstitial positions, the supercell contains 60 Fe atoms and 4 atoms of the solute. The energy was converged in the self-consistent cycle to reduce its fluctuations below 1×10^{-6} eV, forces acting on atoms were relaxed to be smaller than 1×10^{-3} eV/Å, and the stresses were minimized to be less than 0.01 GPa.

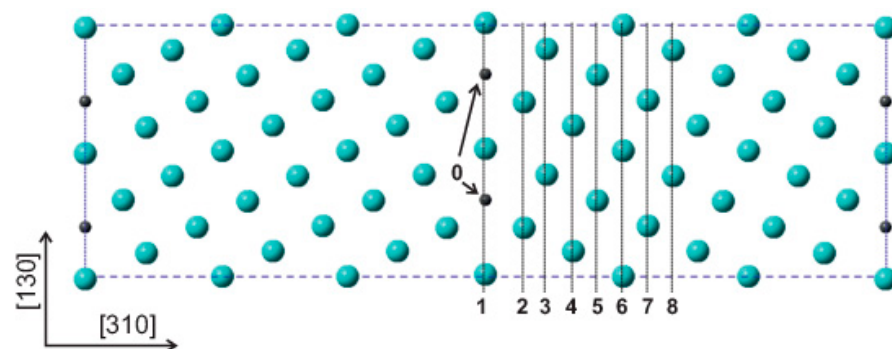


Figure 1. Illustration of the computational supercell with numbered inequivalent atomic planes (starting from the grain boundary). The interstitial positions are labeled as zero. The supercell contains two grain boundaries and we consider the segregation of impurity atoms at both of them to keep the supercell symmetrical.

In order to calculate results for lower concentrations of a solute, one must create a larger simulation supercell which comes with much higher computational demands. For this reason, we employed the machine-learned force fields (MLFF) as implemented in the VASP code (starting from the version 6.3). Therefore, we trained the MLFF for the example of the Fe–Sn system via the on-the-fly ab initio molecular dynamics simulations. The training was performed on a supercell containing 180 atoms (the DFT supercell repeated 3 times along the shortest edge) and the $\Sigma 5$ {310} GB with tin atoms located at substitutional

positions. In the first stage, the system was heated up to 500 K within 5000 steps with the isothermal–isobaric (NpT) ensemble using the Langevin thermostat. After that, the training process continued with another 20,000 steps under constant temperature 500 K. The settings of ab initio molecular dynamics (AIMD) were the same as those for the DFT static simulations mentioned above. The AIMD time step was set to 2 fs. After the training process was finished, we used the generated MLFF for the molecular static simulations on a large supercell containing 2880 atoms ($35.54 \times 28.38 \times 34.67 \text{ \AA}$).

4. Fundamentals of the Comparison of Theoretical and Experimental Results

If we want to compare these two approaches, we must decide what data to use. Principally, we can compare the segregation energies and enthalpies as they differ negligibly at normal pressure [15]. However, it is necessary to average the theoretical data to be comparable with the average segregation energy determined from experiment. Similarly, we can compare the averaged concentrations.

To compare grain boundary concentrations, the calculated data could be averaged according to the White and Coghlan model [21,22]. Supposing simultaneous segregation of the solute to individual sites at a temperature, we can determine the average concentration of I , $X_{I,AVE}^{GB}$, using a combination of the coverages of the solute at individual sites, $\theta_{I,k}^{GB}$, which is defined as [3]:

$$\theta_{I,k}^{GB} = \frac{X_{I,k}^{GB}}{X_k^{GB,0}} \quad (5)$$

considering $X_k^{GB,0}$ to be the concentration at site k in saturation and $X_{I,k}^{GB}$ to be the grain boundary concentration. Accordingly:

$$\theta_{I,AVE}^{GB} = \frac{1}{P} \sum_{k=1}^m \zeta_k \theta_{I,k}^{GB}, \quad (6)$$

where P is the normalization factor, $P = \sum_{k=1}^m \zeta_k$, with ζ_k being the weight of the site, and m is the number of the boundary sites. The coverage of site k can be determined by [21,22]:

$$\theta_{I,k}^{GB} = \frac{X_k^{GB,0} X_I \exp[-(\Delta H_{I,k} - T\Delta S_{I,k})/RT]}{1 - X_I + X_I \exp[-(\Delta H_{I,k} - T\Delta S_{I,k})/RT]}, \quad (7)$$

and the average X_I^{GB} is as follows:

$$X_I^{GB} = \sum \theta_{I,k}^{GB} X_k^{GB,0}. \quad (8)$$

The average theoretical concentrations were determined from the coverages at individual sites (Equation (5)). For the determination of $\theta_{I,k}^{GB}$ (Equation (6)), the value of ΔE_I (published in the literature for individual sites at the grain boundaries) was supplemented by the value of ΔS_I^0 . This value was estimated according to Equation (4) on the basis of models [11,12] with the values of $\Delta S' = +5 \text{ J mol}^{-1} \text{ K}^{-1}$, $\Delta S' = +54 \text{ J mol}^{-1} \text{ K}^{-1}$, for bottom and upper branches, respectively, and $T_{CE} = 900 \text{ K}$ as established for bcc Fe host [23]. Let us note that $\zeta_k = \text{const.}$ Equation (6) was applied in all examples here. This is the simplest possible choice. A more precise approximation can definitely be used. However, $\zeta_k = \text{const.}$ should hold at the compensation temperature T_{CE} ($T_{CE} = 900 \text{ K}$ for bcc iron base systems). The temperature dependence of θ_I^{GB} was constructed from the values of $\theta_{I,k}^{GB}$.

It can be shown that the average energy of the grain boundary segregation, ΔE_I , can be determined from the segregation energies to individual sites, $\Delta E_{I,k}$, analogously to Equation (6):

$$\Delta E_I = \frac{1}{P} \sum_{k=1}^m \zeta_k \Delta E_{I,k}. \quad (9)$$

To determine ΔE_I , we used all sites that provide non-zero values.

Furthermore, we also determined the average values of ΔE_I and ΔS_I from their site counterparts analogously to Equation (6) and then we could compare the averaged experimental and theoretical grain boundary concentrations in the three selected systems, Fe-Si, Fe-V, and Fe-Sn. The system Fe-Si represents the system enabling the direct comparison of the experimental measurements and theoretical calculations at the same {013} grain boundary with an additional comparison to the experimentally based prediction. The system Fe-V compares the experimentally based prediction with the theoretical calculations. In contrast to Si, V exhibits so-called ‘anti-segregation’ sites. Both Si and V solutes correspond to the bottom branch of the enthalpy–entropy compensation effect. The third system, Fe-Sn, which is also considered for comparison, corresponds to the upper branch of the enthalpy–entropy compensation effect. For all selected systems, some experimental data also exist which can be more or less used for documentation of the agreement or disagreement with the prediction or calculation.

5. Comparison of Experimental and Theoretical Data on Grain Boundary Segregation

5.1. System Fe—5 at.% Si

The most interesting systems for our comparison are those providing numerous experimental as well as theoretical data. One of such examples is the segregation of Si at the {013} grain boundary in bcc iron. One can use the data calculated by Jin et al. [24] and results of the experimental study [23] which are listed in Table 1.

Table 1. The average values of ΔH_{Si}^0 and ΔS_{Si}^0 obtained experimentally [23] as well as on basis of prediction [11], and the values of $\Delta E_{Si,k}$ calculated for individual sites [24], all corresponding to the {013} grain boundary of bcc Fe. Values of $\Delta S_{Si,k}$ corresponding to individual $\Delta E_{Si,k}$ were estimated on basis of model [11] (Equation (4)). AES, experimental data; GB site, site according to [24]; PRED, prediction [11]; AVE, average; ΔE_{Si} AVE, average of calculated segregation energies determined according to Equation (9) with $\zeta_k = 1$ and $P = 7$.

GB Site	DFT ΔE_{Si} [24] (kJ mol ⁻¹)	PRED (DFT) ΔS_{Si} [11] (J mol ⁻¹ K ⁻¹)	AES ΔH_{Si} [23] (kJ mol ⁻¹)	AES ΔS_{Si} [23] (J mol ⁻¹ K ⁻¹)	PRED [11] ΔH_{Si}^0 (kJ mol ⁻¹)	PRED [11] ΔS_{Si}^0 (J mol ⁻¹ K ⁻¹)
0	-6.8	-2.5	-	-	-	-
+1, -1	-17.4	-14.3	-	-	-	-
+2, -2	-3.9	+0.7	-	-	-	-
+3, -3	-1	+3.9	-	-	-	-
AVE	-7.3	-3.1	-8	-3	-8.4	-4.4

It is evident that there is an excellent agreement between the experiment and theory in silicon segregation at {013} grain boundary in bcc iron (Figure 2). This system is very simple as the solubility of silicon in bcc iron is extensive and the width of the spectrum of the segregation energies at individual sites is narrow so that this system fits with the bottom branch of the enthalpy–entropy compensation effect [11,12].

5.2. System Fe—2.3 at.% V

The segregation of vanadium was studied at the 46.8°(111) twist grain boundary of bcc Fe by AES [25] and calculated by DFT at the {111} tilt grain boundary by Kholtochina et al. [26]. Although the character of the grain boundaries may be different, we use these data for direct comparison. The data are listed in Table 2 and shown in Figure 3.

It is apparent that both the calculated data [26] and the predictions [11] provide identical temperature dependence of the grain boundary segregation of vanadium at {111} tilt grain boundary of bcc Fe. These dependences also roughly fit with the experimental data (within the error bars) obtained for V segregation at 46.8°(111) twist grain boundary [25]. It is also worth noting that this agreement was obtained by accounting for *all* sites at the grain boundary, i.e., including the ‘anti-segregation’ sites ± 1 (Table 2). This result supports the idea of entropy-dominated grain boundary segregation [27,28].

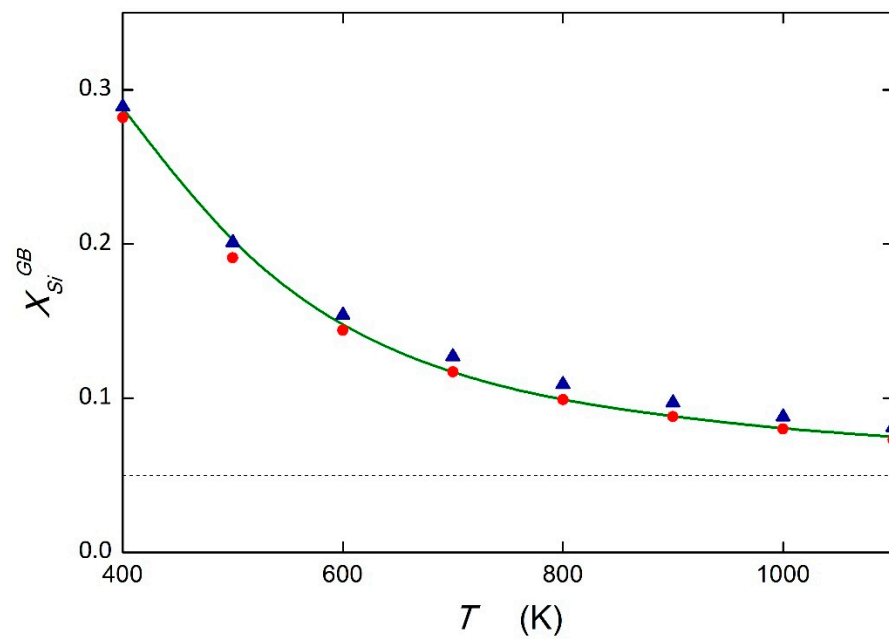


Figure 2. Si concentration at the {013} grain boundary of bcc iron in the temperature range 400–1100 K. The green line represents the averaged concentration obtained from DFT calculations [24], the red points are the values resulting from AES measurements [23], and the blue triangles were estimated on the basis of model [11]. The dotted line corresponds to the bulk concentration, $X_{Si} = 5$ at.%.

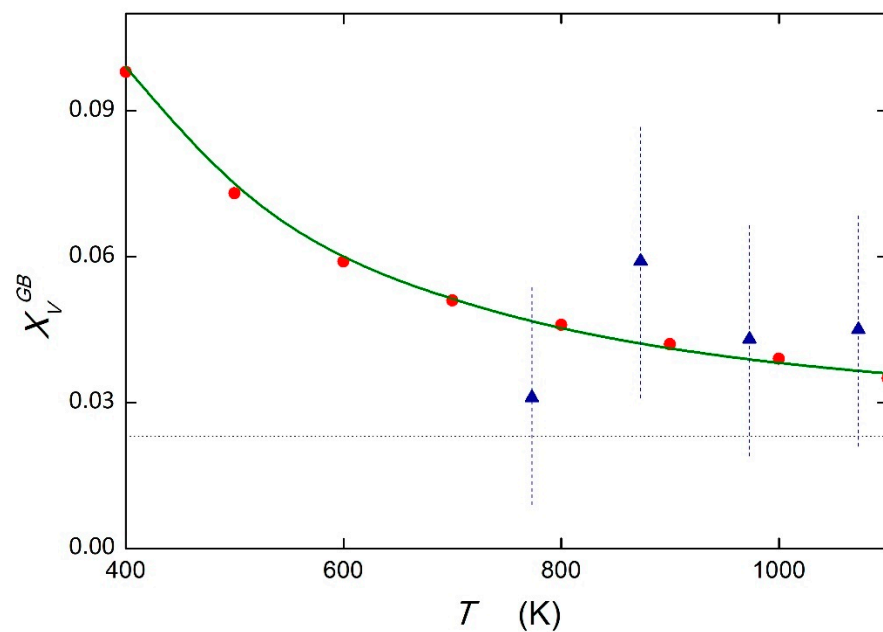


Figure 3. V concentration at the {111} grain boundary of bcc iron in the temperature range 400–1100 K. The green line represents the averaged concentration obtained from DFT calculations [26], the red points are the values resulting from prediction [11] and the blue triangles are experimental data for $46.8^\circ(111)$ twist grain boundary [25]. The dotted line corresponds to the bulk concentration, $X_V = 2.3$ at.%.

Table 2. The average values of ΔH_V^0 and ΔS_V^0 obtained on basis of prediction [11], and the values of $\Delta E_{V,k}$ calculated for individual sites [26], all corresponding to the {111} grain boundary of bcc Fe. Values of $\Delta S_{V,k}$ related to individual $\Delta E_{V,k}$ were estimated on basis of model [11] (Equation (4)). GB site, site according to [26]; PRED, prediction [11]; AVE, average; ΔE_V AVE, average of calculated segregation energies determined according to Equation (9) with $\zeta_k = 1$ and $P = 5$.

GB Site	DFT ΔE_V [26] (kJ mol ⁻¹)	PRED (DFT) ΔS_V [11] (J mol ⁻¹ K ⁻¹)	PRED [11] ΔH_V^0 (kJ mol ⁻¹)	PRED [11] ΔS_V^0 (J mol ⁻¹ K ⁻¹)
0	-16.4	-13.2	-	-
+1, -1	+6.8	+12.5	-	-
+2, -2	-12.5	-8.9	-	-
AVE {111}	-5.6	-1.2	-5.5	-1

5.3. System Fe—0.065 at.% Sn

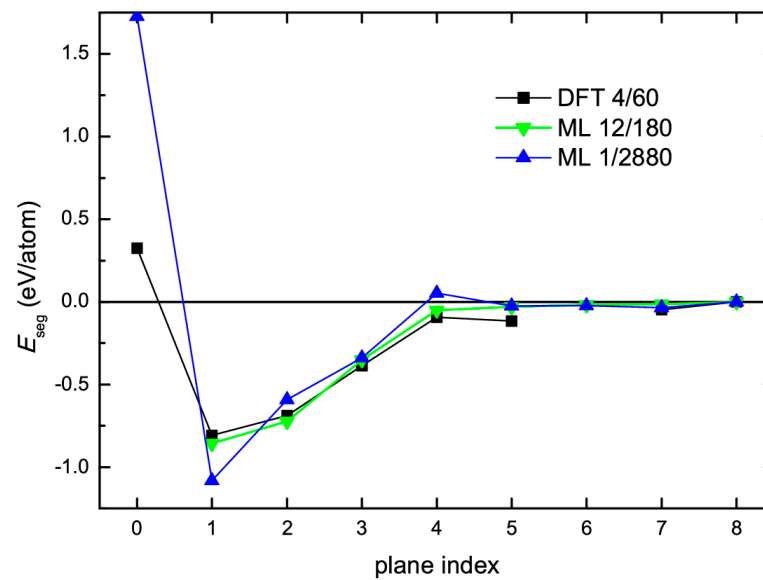
The grain boundary segregation of tin at the grain boundaries of bcc iron was studied by AES in a polycrystalline Fe–0.065 at.%Sn alloy [29]. Even though a spectrum of grain boundaries is measured in polycrystalline material, we can roughly compare these results with our own calculations of the segregation energies to various sites of the {013} grain boundary. As mentioned above, we applied both DFT and ML calculations. Figure 4a shows a benchmark of the computed ML data using the DFT values. The results for 180-atom supercell with 12 impurity atoms can be used for a direct comparison with the energies computed by DFT for a supercell with 60 atoms and four impurity atoms, since both systems have the same impurity concentration. In order to obtain results for smaller concentration of Sn, we created larger supercell (see Figure 4b) with a single impurity atom and 2880 atoms in total. The calculated data on ΔE_{Sn} are listed in Table 3 together with estimated values of ΔS_{Sn} according to the approaches [11,12]. The values of the grain boundary coverage, θ_{Sn}^{GB} , determined by means of these values, are shown in Figure 5.

Table 3. Segregation energy calculated for the segregation of Sn at the {013} grain boundary. GB site, data calculated by ML and DFT in this work (0i, interstitial site, other sites are substitutional); PRED, prediction of ΔS_{Si} according to models [11,12]; AVE, averaged segregation energy according to calculated data for sites determined according to Equation (9) with $\zeta_k = 1$ and $P = 14$ or 12 (according to the number of considered grain boundary sites).

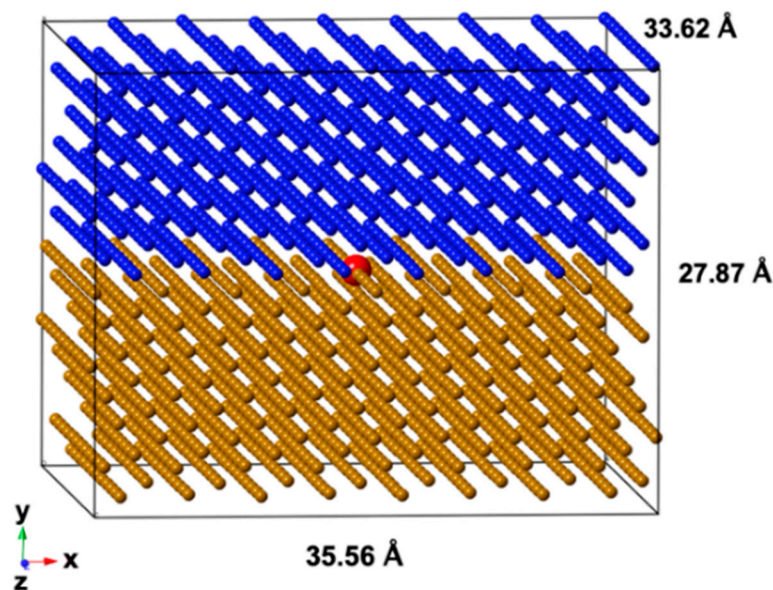
GB Site	ML ΔE_{Sn} (kJ mol ⁻¹)	PRED (ML) ΔS_{Sn} [11] (J mol ⁻¹ K ⁻¹)	PRED (ML) ΔS_{Sn} [12] (J mol ⁻¹ K ⁻¹)	DFT ΔE_{Sn} (kJ mol ⁻¹)	PRED (DFT) ΔS_{Sn} [11] (J mol ⁻¹ K ⁻¹)	PRED (DFT) ΔS_{Sn} [12] (J mol ⁻¹ K ⁻¹)
0i	+166.6	+239.1	+239.1	+31.3	+88.8	+88.8
1	-104.4	-111.0	-62.0	-78.0	-81.7	-32.7
+2, -2	-57.1	-58.5	-9.5	-66.5	-68.9	-19.9
+3, -3	-32.6	-31.2	+17.8	-37.2	-36.3	+12.7
+4, -4	+5.1	+10.7	+59.7	-9.0	-5.0	+44.0
+5, -5	-2.3	+2.4	+51.4	-11.2	-7.4	+41.6
+6, -6	-2.3	+2.4	+51.4	-	-	-
+7, -7	-3.5	+1.1	+50.1	-4.5	0	49.0
AVE ΔS_{Si} [11]	-8.8	-1.3	-	-25.3	-19.0	-
AVE ΔS_{Si} [12]	-8.8	-	+44.2	-25.3	-	+25.9
PRED [11]	-7	-	+46	-7	-	+46

The Fe-Sn system exhibits a wide spectrum of the segregation energies in contrast to the previous systems, Fe-Si and Fe-V. Consequently, many more sites (including the interstitial one) provide non-zero values of the segregation energy. Therefore, all of them must be considered in averaging ΔE_T according to Equation (9). It is worth noting that the value of $\Delta E_{Sn} = -8.8$ kJ mol⁻¹ calculated on basis of ML approach is very close to $\Delta H_{Sn}^0 = -8.0$ kJ mol⁻¹ predicted in [11]. On the other hand, the value of $\Delta E_{Sn} = -25.3$ kJ mol⁻¹ calculated by the DFT approach differs considerably from the above values. However, the value of $\Delta S_{Sn} = -1.3$ J mol⁻¹ K⁻¹ estimated according to model [11] for the formerly calculated $\Delta E_{Sn} = -8.8$ kJ mol⁻¹ differs

from the prediction. The reason is that the entropies for the substitutional sites were estimated using the bottom branch of Equation (4) and that for the single interstitial site was taken from the upper branch. In contrast to that, only the upper branch was considered in the prediction. Nevertheless, the value of ΔS_{Sn} estimated according to model [12], i.e., using only the upper branch, fits well with the prediction [11].



(a)



(b)

Figure 4. (a) Segregation energy computed using DFT and ML. The legend also contains the number of solute atoms and the total number of atoms in the supercell. (b) Illustration of the computational supercell with 2880 atoms and a single substitutional impurity atom in the GB plane.

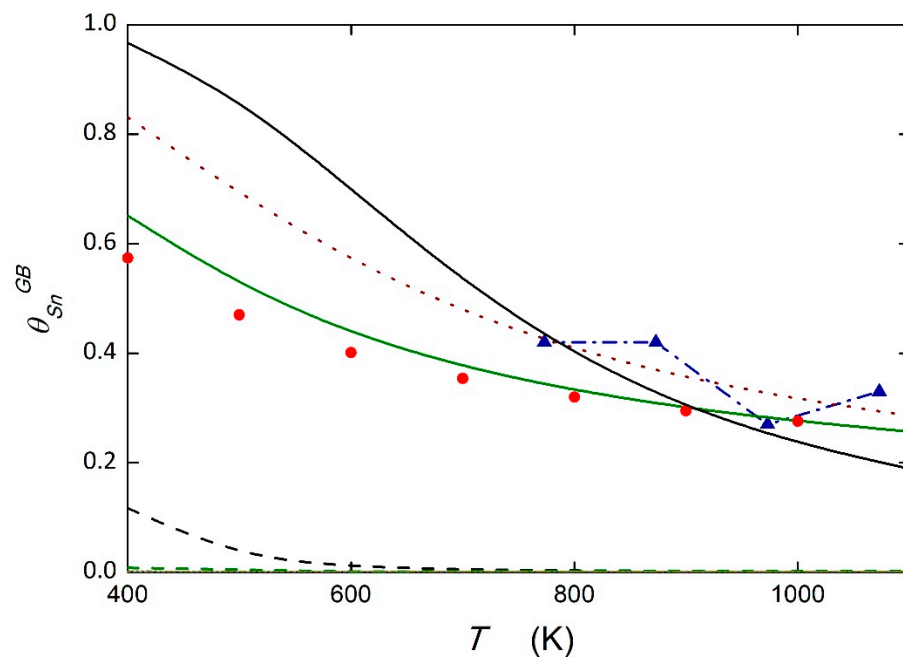


Figure 5. Sn concentration at the {013} grain boundary of bcc iron in the temperature range 400–1100 K. The red points are the values resulting from prediction [11]. The full lines represent the averaged concentration obtained from ML (green) and DFT (black) calculations with ΔS_{Sn} determined according to [12], and the dashed lines represent the respective calculations with ΔS_{Sn} determined according to [11]. The blue triangles are experimental data measured in a polycrystalline Fe–0.065 at% Sn alloy [25].

ΔE_{Sn} and Sn coverages determined by DFT differ substantially from the prediction regardless of the model used to estimate ΔS_{Sn} . These conclusions are well visible in Figure 5. Here, the coverages are compared to the grain boundary coverages measured in polycrystalline Fe–0.065 at.% Sn alloy [12]. We can see that the data based on prediction [11] as well as the data calculated by ML with ΔS_{Sn} estimated by model [12] agree better with the experiment than the data determined by DFT, although the latter seem to fit with the experimental data too. However, we must keep in mind that highly segregated general grain boundaries are measured by AES at temperatures below compensation temperature (900 K) which possess higher solute concentrations than the special boundaries, such as the {013} grain boundary. On the contrary, the special boundaries are more segregated above the compensation temperature [29,30] and we see much better agreement of the prediction and ML calculations with experimental data in this temperature region (Figure 5). It is also worth noting that Seah and Lea [31] describe the Sn segregation by the values $\Delta H_{Sn} = -13.1 \text{ kJ mol}^{-1}$ and $\Delta S_{Sn} = +41.5 \text{ J mol}^{-1} \text{ K}^{-1}$ corresponding to general grain boundaries. The corresponding temperature dependence of the tin coverage is depicted by the dotted dark-red line in Figure 5. These coverages fit very well with the experimental data and are higher than those determined for the {013} grain boundary by ML, which justifies the larger segregation at general grain boundaries as compared to that at the special ones. On the other hand, they are lower than those calculated by DFT, which supports the conclusion that ML calculations reflect tin segregation more accurately.

6. Discussion

As was mentioned in Introduction, there is lack of a direct comparison of grain boundary segregation obtained from experimental data and calculated results. For this comparison, it is necessary to fulfill several conditions. One of them is a satisfactory solid solubility of the segregant in the bulk of the host [10]. High solid solubility, however, results in low segregation of the solute at the grain boundaries and thus also usually in good grain boundary cohesion [9], which is disadvantageous for AES measurements

performed on fractured grain boundaries [6]. Nevertheless, such data can also be found in the literature and here we can make such comparison for three selected systems exhibiting high solid solubility.

The grain boundary segregation of Si in bcc Fe was measured in a P-containing system but the data for Si segregation at grain boundaries in the binary Fe–Si system can be drawn from the complex segregation data enabling the determination of $\Delta H_{Si} = -8 \text{ kJ mol}^{-1}$ and $\Delta S_{Si} = -3 \text{ J mol}^{-1} \text{ K}^{-1}$ for the {013} tilt grain boundary [23]. Calculations for this grain boundary were performed by Jin et al. [24]. The calculated average value of $\Delta E_{Si} = -7.3 \text{ kJ mol}^{-1}$ is in excellent agreement with the above value of the experimental ΔH_{Si} and, therefore, the values of ΔS_{Si} are nearly identical. All these data are also in very good agreement with the prediction [11], $\Delta H_{Si} = -8.4 \text{ kJ mol}^{-1}$ and $\Delta S_{Si} = -4.4 \text{ J mol}^{-1} \text{ K}^{-1}$ (Table 1). The corresponding grain boundary concentrations at different temperatures show outstanding agreement (Figure 2).

Very good agreement was also found between our experimental prediction and theoretical data on grain boundary segregation of V in bcc Fe. Even in this case, the data were obtained in a ternary system containing phosphorus [25]. Although the scatter of the data is quite large at the $46.8^\circ(111)$ twist grain boundary (Figure 2), the data agree well with both the prediction $\Delta H_V = -5.5 \text{ kJ mol}^{-1}$ and $\Delta S_V = -1 \text{ J mol}^{-1} \text{ K}^{-1}$ [11] and with the data for the {111} tilt grain boundary $\Delta E_V = -5.6 \text{ kJ mol}^{-1}$ calculated by Kholtochina et al. [26] (for which the value $\Delta S_{Si} = -1.2 \text{ J mol}^{-1} \text{ K}^{-1}$ was estimated [11], see Table 2). However, this agreement was obtained only if the data on segregation energy were used for all sites, i.e., including the ‘anti-segregation’ ones with positive values of the segregation energy. If only the sites with negative segregation energy are considered, the value of $\Delta E_V = -13.8 \text{ kJ mol}^{-1}$ is nearly three times higher. This supports the idea of entropy-driven grain boundary segregation [32], suggesting that the grain boundary can be enriched in the case of $\Delta E_I > 0$ if $T\Delta S_I > \Delta E_I > 0$.

In the previous cases, the grain boundary saturation was equal to 1 and there was no difference between X_I^{GB} and θ_I^{GB} . However, in the system Fe–Sn, the saturation of the boundary is lower, $X_k^{GB,0} = 1/3$, and we must distinguish between these two quantities. Therefore, θ_{Sn}^{GB} is plotted in Figure 5. In contrast to the previous two systems, in which substitutional segregation is expected and the value of ΔS_I was unambiguously estimated using the bottom branch of the enthalpy–entropy compensation effect (Equation (4)), here the experimental data fit with the upper branch supposed to correspond to interstitial segregation. We see in Figure 5 that the prediction [11] fits well with the experimental points if we keep in mind that, in polycrystalline material, the general boundaries are open during the brittle fracture after annealing at temperatures below the compensation temperature. However, at higher temperatures, the special boundaries are more segregated, and it is probable that they will appear more frequently at the fracture surface [29,30]. The agreement of the experimental data and our prediction at higher temperatures is then very good and higher concentrations of Sn at lower temperatures compared to the prediction for the {013} grain boundary reflect the different characters of the grain boundaries studied (Figure 5).

The prediction of tin grain boundary segregation can also be compared with our own calculated data. These data were obtained from both the DFT calculations and the ML treatment. It is remarkable that the value $\Delta E_{Sn} = -8.8 \text{ kJ mol}^{-1}$ obtained from ML is very close to the predicted value $\Delta H_{Sn} = -7 \text{ kJ mol}^{-1}$. However, the application of the substitutional and interstitial branches to estimate ΔS_{Sn} for respective sites provides the value $\Delta S_{Sn} = -1.3 \text{ J mol}^{-1} \text{ K}^{-1}$ which differs substantially from the predicted $\Delta S_{Sn} = +46 \text{ J mol}^{-1} \text{ K}^{-1}$. The corresponding temperature dependence of the grain boundary coverage (green dashed line in Figure 5) then differs substantially from that resulting from application of the prediction [9]. However, the application of the approach of Scheiber and Romaner [12], which suggested that the upper branch describes the segregation entropy of the systems possessing a wide spectrum of the segregation energies, provides a

reasonable value $\Delta S_{Sn} = +44.2 \text{ J mol}^{-1} \text{ K}^{-1}$, which results in a temperature dependence nearly identical with the predicted one (green full line in Figure 5).

The data calculated using the DFT approach provide us with the average value of $\Delta E_{Sn} = -25.3 \text{ kJ mol}^{-1}$ which is more than three times higher (in absolute value) than the predicted as well as the ML calculated values. Accordingly, the predicted values of ΔS_{Sn} differ from the predicted ones as well as from the ML calculations, even though the upper branch [12] or particularly the upper and the bottom branches [11] were used. However, the temperature dependence of the Sn concentration with ΔS_{Sn} estimated according to model [12] (black full line in Figure 5) seems to be reasonable in respect to the experimental data. However, we must keep in mind that experimental data were determined by measurements on a polycrystalline Fe-Sn alloy with an undefined spectrum of grain boundaries. It is justifiable that they are mainly of general character, thus generally possessing higher absolute values of the segregation energy/enthalpy which are hardly comparable with those of the $\Sigma 5$ special boundary. Their realistic correlation by the former approach is more probable due to the difference in the character of the boundaries studied and in degree of agreement with the prediction philosophy [11]. Nevertheless, the approach of Scheiber and Romaner [12] seems to refine the understanding of the enthalpy–entropy compensation effect.

7. Conclusions

In this paper, the experimental grain boundary concentrations at different temperatures are compared to both the theoretical calculations and our prediction [9] for three bcc-Fe based systems characterized by satisfactory solid solubility in the bulk. This comparison provides the following important conclusions:

- An excellent agreement between experiment and calculation can be obtained when the solid solubility of the solute is high enough, i.e., well above 1 at.%;
- Experimental and calculated data can be compared on basis of averaged values of the segregation energy;
- Averaged values of the segregation energy must be determined using all sites, including the ‘anti-segregation’ ones;
- To predict the value of the segregation entropy, the approach of Scheiber and Romaner [12] distinguishing the upper and bottom branches of the enthalpy–entropy compensation effect seems to be valuable.

Author Contributions: Conceptualization, P.L.; Formal analysis, M.V.; Funding acquisition, M.Č.; Investigation, P.Š. and M.V.; Methodology, M.Č., P.Š. and P.L.; Project administration, M.Č.; Visualization, M.Č.; Writing—original draft, P.L.; Writing—review & editing, M.Č. and P.Š. All authors have read and agreed to the published version of the manuscript.

Funding: This research was funded by the Czech Science Foundation (Project No. GA-20-08130S), P.L. also acknowledges financial support by the Academy of Sciences of the Czech Republic (RVO:68378271).

Institutional Review Board Statement: Not applicable.

Informed Consent Statement: Not applicable.

Data Availability Statement: This article has no additional data. All data included in this study are available upon request by contact with the corresponding author.

Acknowledgments: Computational resources were provided by the Ministry of Education, Youth and Sports of the Czech Republic under the Projects e-INFRA CZ (ID:90140) at the IT4Innovations National Supercomputing Center.

Conflicts of Interest: The authors declare that there is no known competing financial interest or personal relationships that could have appeared to influence the work reported in this paper.

References

1. Briant, C.L. (Ed.) *Impurities in Engineering Materials, Impact, Reliability and Control*; Marcel Dekker, Inc.: New York, NY, USA, 1999.
2. Flewitt, P.E.J.; Wild, R.K. *Grain Boundaries, Their Microstructure and Chemistry*; John Wiley and Sons, Ltd.: Chichester, UK, 2001.
3. Lejček, P. *Grain Boundary Segregation in Metals*; Springer: Berlin/Heidelberg, Germany, 2010.
4. McLean, D. *Grain Boundaries in Metals*; Clarendon Press: Oxford, UK, 1957.
5. Hondros, E.D. Grain Boundary Segregation Assessment of Investigative Techniques. In *Grain Boundary Structure and Properties*; Chadwick, G.A., Smith, D.A., Eds.; Academic Press: London, UK, 1976; pp. 265–298.
6. Hofmann, S. Auger and X-ray Photoelectron Spectroscopy in Materials Science. In *A User-Oriented Guide*; Springer: Berlin/Heidelberg, Germany, 2013.
7. Kuzmina, M.; Ponge, D.; Raabe, D. Grain Boundary Segregation Engineering and Austenite Reversion Turn Embrittlement into Toughness: Example of a 9 wt.% Medium Mn Steel. *Acta Mater.* **2015**, *86*, 182–192. [[CrossRef](#)]
8. Amram, D.; Schuh, C.A. Interplay Between Thermodynamic and Kinetic Stabilization Mechanisms in Nanocrystalline Fe-Mg alloys. *Acta Mater.* **2018**, *144*, 447–458. [[CrossRef](#)]
9. Lejček, P.; Šob, M.; Paidar, V. Interfacial Segregation and Grain Boundary Embrittlement: An Overview and Critical Assessment of Experimental Data and Calculated Results. *Prog. Mater. Sci.* **2017**, *87*, 83–139. [[CrossRef](#)]
10. Lejček, P.; Šob, M.; Paidar, V.; Vitek, V. Why Calculated Energies of Grain Boundary Segregation Are Unreliable When Segregant Solubility Is Low. *Scripta Mater.* **2013**, *68*, 547–550. [[CrossRef](#)]
11. Lejček, P.; Hofmann, S. Modeling Grain Boundary Segregation by Prediction of All the Necessary Parameters. *Acta Mater.* **2019**, *170*, 253–267. [[CrossRef](#)]
12. Scheiber, D.; Romaner, L. Impact of the Segregation Energy Spectrum on the Enthalpy and Entropy of Segregation. *Acta Mater.* **2021**, *221*, 117393. [[CrossRef](#)]
13. Lejček, P. Characterization of Grain Boundary Segregation in Fe-Si Alloy. *Anal. Chim. Acta* **1994**, *297*, 165–178. [[CrossRef](#)]
14. Hondros, E.D.; Seah, M.P. Segregation to Interfaces. *Int. Met. Rev.* **1977**, *22*, 262–299. [[CrossRef](#)]
15. Lejček, P.; Zheng, L.; Hofmann, S.; Šob, M. Applied Thermodynamics: Grain Boundary Segregation. *Entropy* **2014**, *16*, 1462–1483. [[CrossRef](#)]
16. Lejček, P.; Hofmann, S. Thermodynamics of Grain Boundary Segregation and Applications to Anisotropy, Compensation Effect and Prediction. *Crit. Rev. Sol. State Mater. Sci.* **2008**, *33*, 133–163. [[CrossRef](#)]
17. Kresse, G.; Hafner, J. Ab Initio Molecular Dynamics for Open-Shell Transition Metals. *Phys. Rev. B* **1993**, *48*, 13115. [[CrossRef](#)] [[PubMed](#)]
18. Kresse, G.; Furhüller, J. Efficient Iterative Schemes for Ab Initio Total-Energy Calculations Using a Plane-Wave Basis Set. *Phys. Rev. B* **1996**, *54*, 11169–11186. [[CrossRef](#)] [[PubMed](#)]
19. Kresse, G.; Joubert, D. From Ultrasoft Pseudopotentials to the Projector Augmented-Wave Method. *Phys. Rev. B* **1999**, *59*, 1758–1775. [[CrossRef](#)]
20. Perdew, J.P.; Burke, K.; Ernzerhof, M. Generalized Gradient Approximation Made Simple. *Phys. Rev. Lett.* **1996**, *77*, 3865–3868. [[CrossRef](#)] [[PubMed](#)]
21. White, C.L.; Coghlan, W.A. The Spectrum of Binding Energies Approach to Grain Boundary Segregation. *Metall. Trans. A* **1977**, *8*, 1403–1412. [[CrossRef](#)]
22. Nowicki, T.; Joud, J.C.; Biscondi, M. A Thermodynamic Model of Grain Boundary Segregation for Atomistic Calculations. *J. Phys. Colloq.* **1990**, *51*, C1-293–C1-298. [[CrossRef](#)]
23. Lejček, P.; Hofmann, S. Interstitial and Substitutional Solute Segregation at Individual Grain Boundaries of α -Iron: Data Revisited. *J. Phys. Condens. Matter.* **2016**, *28*, 064001. [[CrossRef](#)]
24. Jin, H.; Elfimov, I.; Militzer, M. Study of the interaction Of Solutes With $\Sigma 5$ (013) Tilt Grain Boundaries in Iron Using Density-Functional Theory. *J. Appl. Phys.* **2014**, *115*, 093506. [[CrossRef](#)]
25. Lejček, P.; Pokluda, J.; Šandera, P.; Horníková, J.; Jenko, M. Solute Segregation At 46.8 (111) Twist Grain Boundary of a Phosphorus Doped Fe–2.3%V Alloy. *Surface Sci.* **2012**, *606*, 258–262. [[CrossRef](#)]
26. Kholobina, A.S.; Ecker, W.; Pipan, R.; Razumovskiy, V.I. Effect of Alloying Elements on Hydrogen Enhanced Decohesion in Bcc Iron. *Comput. Mater. Sci.* **2021**, *188*, 110215. [[CrossRef](#)]
27. Lejček, P.; Hofmann, S.; Všíanská, M.; Šob, M. Entropy Matters in Grain Boundary Segregation. *Acta Mater.* **2021**, *206*, 116597. [[CrossRef](#)]
28. Lejček, P.; Hofmann, S. Entropy-dominated grain boundary segregation. *J. Mater. Sci.* **2021**, *56*, 7464–7473. [[CrossRef](#)]
29. Lejček, P.; Šandera, P.; Horníková, J.; Pokluda, J.; Godec, M. On the Segregation Behavior of Tin and Antimony at Grain Boundaries of Polycrystalline Iron. *Appl. Surf. Sci.* **2016**, *363*, 140–144. [[CrossRef](#)]
30. Lejček, P.; Jäger, A.; Gärtnerová, V. Reversed Anisotropy of Grain Boundary Properties and Its Effect on Grain Boundary Engineering. *Acta Mater.* **2010**, *58*, 1930–1937. [[CrossRef](#)]
31. Seah, M.P.; Lea, C. Surface Segregation and Its Relation to Grain Boundary Segregation. *Philos. Mag.* **1975**, *31*, 627–645. [[CrossRef](#)]
32. Lejček, P.; Hofmann, S. Entropy-Driven Grain Boundary Segregation: Prediction of the Phenomenon. *Metals* **2021**, *11*, 1331. [[CrossRef](#)]